Porites Calcifying Fluid pH on Seasonal to Diurnal Scales

Oliver Knebel[1], Carlos Carvajal[1], Christopher D. Standish[2], Elwyn de la Vega[2], Thomas B. Chalk[2], Emma J. Ryan[1], Weifu Guo[3], Murray Ford[1], Gavin L. Foster[2], and Paul Kench[4]

[1]School of Environment, University of Auckland, Auckland, New Zealand. [2]School of Ocean and Earth Science, University of Southampton, Southampton, United Kingdom. [3]Department of Geology and Geophysics, Woods Hole Oceanographic Institution, Woods Hole, MA, USA. [4]Department of Earth Sciences, Simon Fraser University, Burnaby, BC, Canada.

Corresponding author: Oliver Knebel (okne620@aucklanduni.ac.nz)

Key Points:

- *Porites* calcifying fluid pH was investigated using conventional and laser ablation boron isotope analysis, and a calcification model
- On a seasonal scale, *Porites* calcifying fluid pH followed mainly seawater temperatures that control calcification rates
- On a diurnal scale, model estimates suggest limited calcifying fluid pH variability despite highly variable reef flat seawater conditions

Abstract

Coral resilience to ocean acidification is largely determined by the degree of physiological control corals can exert on their calcifying fluid carbonate chemistry. In this study, the boron isotopic composition ($\delta^{11}B$) of a *Porites* colony growing on a reef flat on Kiritimati Island in the equatorial central Pacific is examined to quantify the sensitivity of calcifying fluid pH (pH_{cf}) to ambient environmental conditions. Skeletal $\delta^{11}B$ along the growth axis of one annual growth band was determined with bulk analysis and by laser ablation (LA) MC-ICP-MS. Furthermore, the oxygen and carbon isotopic composition, trace element ratios, and skeletal density was quantified. Sclerochronological data were interpreted in the context of simultaneous recordings of reef flat seawater pH (pH_{sw}), temperature, salinity, and water depth, and by measurements of these parameters on the fore-reef. A recent model of pH_{cf} upregulation, after optimization with seasonally resolved data, was used to simulate pH_{cf} variability on a diurnal scale. Results showed that on a seasonal scale, *Porites* pH_{cf} is upregulated compared to ambient seawater: both bulk and LA-MC-ICP-MS derived $\delta^{11}B$ resulted in a mean pH_{cf} of 8.35 pH units. Calcifying fluid pH upregulation primarily followed variations in seawater temperatures that is likely related to the control of temperature on calcification rate. On the reef flat, the diurnal range in pH_{sw} was substantially higher (0.29 pH units) than on the fore-reef (0.07 pH units). However, model results suggest that the high diurnal variability in reef flat pH_{sw} had only a limited effect on the variability in *Porites* pH_{cf}.

Plain Language Summary

Ocean acidification and the associated decline in seawater pH has impacted the ability of many marine organisms to calcify. However, tropical corals do not precipitate their aragonite skeletons from seawater, but instead from a calcifying fluid located between skeleton and living tissue. The chemistry of this calcifying fluid is modified by physiological processes. This study examines the sensitivity of the calcifying fluid pH to variations in environmental conditions. Seawater pH, temperature, salinity, and water depth on a reef flat at Kiritimati Island in the central Pacific were monitored for one year. The calcifying fluid pH of a synchronously precipitated annual growth band of a *Porites* colony was determined using boron isotope analysis with dissolution of samples and novel laser ablation at enhanced resolution. Furthermore, a numerical model predicted calcifying fluid pH variability at a diurnal scale based on the environmental and

geochemical data collected. Results indicate that on a seasonal scale, seawater temperatures rather than seawater pH control the calcifying fluid pH. Further geochemical analysis suggests that this is related to the temperature dependency of the calcification rate. On a diurnal scale, model results suggest no elevated variability in calcifying fluid pH despite highly variable reef flat seawater conditions.

1 Introduction

Atmospheric CO_2 levels have increased dramatically since the beginning of the industrial era, with one-quarter of the emitted CO_2 being absorbed by the oceans (Friedlingstein et al., 2019). This process, known as ocean acidification (OA), has lowered pH_{sw} by approximately 0.1 pH units compared to the preindustrial and reduced the seawater saturation state of the biologically important carbonate minerals calcite and aragonite (Ω_{sw}; Bindoff et al., 2019). Ocean acidification is a significant environmental stressor for marine life as it is thought to affect the ability of many organisms to calcify. However, in coastal environments, such as coral reefs, pH_{sw} is not only controlled by atmospheric CO_2 but also is influenced by multiple drivers including tidal (Bates et al., 2010; Cyronak et al., 2018) and ecosystem-level processes (Smith, 1973; Gattuso et al., 1993; DeCarlo et al., 2017). Thus, the effect of OA on coastal environments is more complex and less predictable than in the open ocean (Duarte et al., 2013). Furthermore, corals do not precipitate $CaCO_3$ directly from seawater, but instead from a medium located between calicoblastic cell membrane and skeleton, that is often referred to as calcifying fluid (Gattuso et al., 1999). Enzymatic processes elevate pH_{cf} relative to ambient pH_{sw} to facilitate aragonite precipitation (Constantz, 1986; McCulloch et al., 2017; Sevilgen et al., 2019). Thus, corals may exhibit some resilience to OA by upregulating pH_{cf} (McCulloch et al., 2012). However, despite laboratory experiments showing pH_{cf} correlates with pH_{sw} (Hönisch et al., 2004; Krief et al., 2010; Venn et al., 2011), the sensitivity of coral pH_{cf} to changes in ambient pH_{sw} in natural environments is still unclear with some studies arguing that *Porites* corals maintain nearly constant pH_{cf} despite variable ambient pH_{sw} (i.e. pH_{cf} homeostasis; Georgiou et al., 2015; Comeau et al., 2019), while others find pH_{cf} is partially controlled by pH_{sw} (D'Olivo et al., 2019; Guo, 2019) or that pH_{cf} follows predominantly changes in pH_{sw} (Kubota et al., 2017). Most of these studies have analyzed *Porites* calcifying fluid carbonate chemistry variability on

inter-decadal or seasonal time scales and only a few have focussed on shorter time scales, such as the diurnal variability (Cornwall et al., 2018; DeCarlo et al., 2019).

The main objective of this study is to quantify the sensitivity of pH_{cf} upregulation to ambient seawater conditions in *Porites*, a coral genus that can be found on reef flats where pH_{sw} naturally varies on both seasonal and diurnal scales. In this study, as in many others (Hönisch et al., 2004; Krief et al., 2010; Georgiou et al., 2015; Kubota et al., 2017; D'Olivo et al., 2019), the boron isotope ratio ($\delta^{11}B$) of skeletal $CaCO_3$ is used to infer pH_{cf} (McCulloch et al., 2018). To explore pH_{cf} variability on a sub-monthly scale, variations of $\delta^{11}B$ are measured along the growth axis of one year of growth of a *Porites* sp. colony using laser ablation (LA) multi-collector inductively coupled plasma mass spectrometry (MC-ICP-MS; Standish et al., 2019). The data are coupled with measurements of other sclerochronological tracers, such as oxygen and carbon isotopes ($\delta^{18}O/\delta^{13}C$), conventional $\delta^{11}B$ analysis with dissolution of samples (bulk), trace elements, and skeletal density. Calcifying fluid pH and other carbonate system parameters are calculated from coral $\delta^{11}B$ and B/Ca, and their sensitivity to changes in ambient pH_{sw}, temperature, and salinity are quantified. Furthermore, to estimate pH_{cf} variability on a diurnal scale, a recent model that simulates coral pH_{cf} upregulation from ambient environmental conditions (Guo, 2019) is applied. The model is optimized using seasonally resolved geochemical and instrumental data from this study and subsequently used to estimate pH_{cf} variability on a diurnal scale from half-hourly resolved instrumental data.

2 Materials and Methods

2.1 Study Site

Kiritimati Island is a coral atoll in the equatorial central Pacific located at 1.9°N 157.4°W (Fig. 1) where inter-annual climate variability is dominated by the El Niño Southern Oscillation (Cobb et al., 2003) and ocean pH_{sw} is one of the lowest in the Pacific at approximately 8.0 (Bakker et al., 2016). Average annual sea surface temperatures (SST) vary between 24°C during La Niña and 30°C during El Niño conditions (Woodroffe et al., 2003), and average rainfall rates are low, averaging 900 mm/year (1951–2006) and increase up to 3000 mm/year during El Niño events (Morrison & Woodroffe, 2009). El Niño events also cause a pronounced positive sea level anomaly of up 0.3 m compared to La Niña conditions (Woodroffe et al., 2012). The tides at Cecile Peninsula follow a semi-diurnal cycle with a maximal tidal range of 1.12 m. Kiritimati

105 Island has been chosen as a study site due to its location close to the equator where the seasonal
106 variability in environmental parameters, such as seawater temperature, is expected to be small,
107 facilitating quantification of the effect of pH_{sw} on pH_{cf} upregulation. The study was conducted on
108 Cecile Peninsula (Fig. 1, coordinates of sampling sites see table S1 and S2) located in the South
109 of Kiritimati Island with only minor human influence (Walsh, 2011).

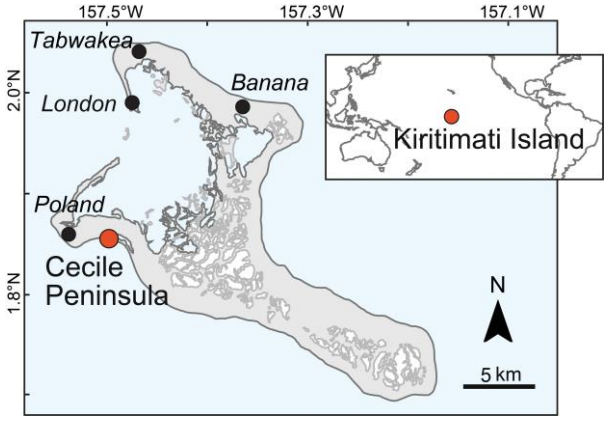

Figure 1. Map of Kiritimati Island with the location of the study site (Cecile Peninsula) and settlements. Also shown is the location of Kiritimati Island in the Pacific Ocean.

110 2.2 Environmental Monitoring

111 A 110 cm diameter microatoll colony of *Porites* sp. (Scoffin et al., 1978; Kench et al., 2019) on
112 the central reef flat at Cecile Peninsula was treated with alizarin red S (Lamberts, 1978) for 24
113 hours on the 14th May 2017, and was collected after approximately one year of growth on the
114 25th May 2018. The treatment provided a red marker in the coral skeleton enabling detection and
115 subsequent sampling of one year of $CaCO_3$ deposition (Fig. 2a).

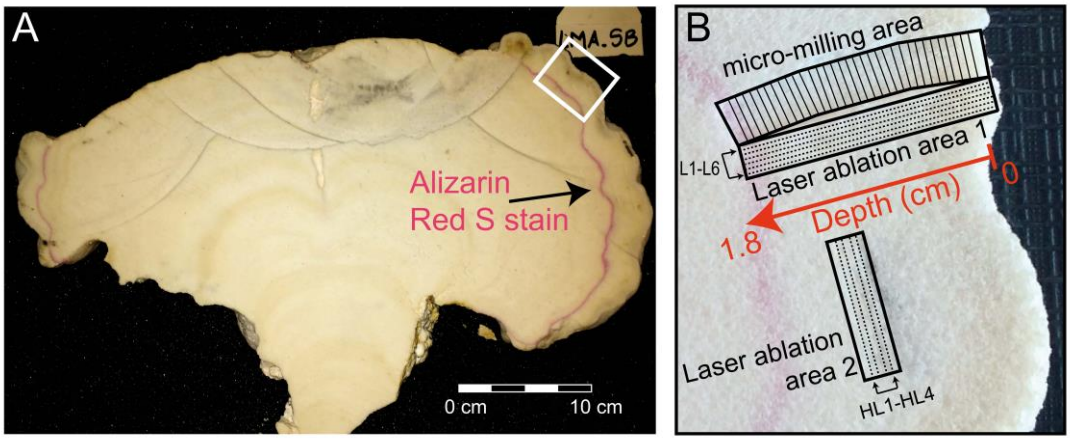

Figure 2. Section of *Porites* sp. colony with distinct red alizarin red S stain band (a). Areas in the annual growth layer analyzed: In the *micro-milling area* samples were removed with a micro-mill and dissolved prior to analysis (bulk analysis). In laser ablation area 1 (LAA-1) and 2 (LAA-2), material was analyzed in situ with LA-MC-ICP-MS (b).

Located 27 m from the stained coral, a sensor package consisting of a SeaFET pH-sensor and CTD logger was deployed over the same period at approximately 0.5–1 m depth relative to mean sea level. The sensor package measured pH_{sw}, temperature, salinity, and water depth (pressure) at 30 min intervals. Flooding of the SeaFET pH-sensor caused a gap in the pH_{sw} data between the 6th September 2017 and 9th March 2018 when the damaged SeaFET pH-sensor was replaced by an identical model. Measurements of pH_{sw} from the external SeaFET pH electrode were corrected for temperature and salinity using measurements from the CTD logger following Martz et al. (2010) and Miller et al. (2018). To evaluate differences in environmental conditions between reef flat and fore-reef, the sensor package was subsequently deployed on Cecile Peninsula fore-reef for 9 days between the 28th of May and the 5th of June 2018 at approximately 7 m depth relative to mean sea level. For determination of the total alkalinity of seawater (TA_{sw}), seawater samples were collected from the reef flat in September 2017 and May 2018, and from the fore-reef in May 2018 (Table S1 in the Supplement). Seawater samples were collected during the day and night following Dickson et al. (2007). Titration of seawater samples to determine the TA_{sw} was performed at the University of Otago in Dunedin, New Zealand. A portable pH-meter Orion A325 calibrated with TRIS and AMP buffer solutions was used for measurements of pH_{sw}, temperature, and salinity accompanying TA_{sw} sampling. All pH-measurements of this study are

indicated on the total scale. Time series analysis of environmental data was conducted in R (R Core Team, 2019).

2.3 Sample Preparation, X-ray Densitometry, SEM

At the end of the one-year growth experiment, the stained coral was cut with a saw, cleaned, and treated with sodium hypochlorite overnight. The specimen was later cut into 7 mm thick slices using a diamond wet saw. A micro-mill with a 1 mm diameter drill bit was then used to extract 34 sequential samples of 0.5–3.5 mg of $CaCO_3$ from the annual growth band. Of these samples, 32 covered 0.5 mm, and 2 covered 1.0 mm of coral growth along the 1.8 cm long growth axis from the alizarin-stained band to the edge of the coral (Fig. 2b). Thus, one sample represents on average 11 days of calcification. Variations of skeletal density within the annual growth band were calculated from X-ray images (Carricart-Ganivet & Barnes, 2007) recorded at Mercy Radiology Auckland, New Zealand (Fig. S1 in the Supplement). For this purpose, 7 mm thick cubes of coral aragonite with known density were used as standards enabling calibration of the X-ray image's greyscale against discrete density values using the program R (R Core Team, 2019). This was done for the area sampled by micro-milling (micro-milling area) and laser ablation area 1 (LAA-1) analyzed by LA-MC-ICP-MS.

2.4 Geochemical Analysis

A subsample of 0.05–0.07 mg $CaCO_3$ was taken from the 34 micro-milled samples for $\delta^{18}O$ and $\delta^{13}C$ analyses at the Stable Isotope Mass Spectrometry Laboratory of the University of Southampton (UK). The remaining sample material was oxidatively cleaned by treatment with 30% H_2O_2 buffered with ~0.1 M NH_4OH and dissolved in ~0.15 M HNO_3. Ten of the dissolved samples were then split into subsamples to permit trace element analysis (~10%) and boron isotope analysis (~90%). Both analyses were carried out at the University of Southampton. Trace element analysis (Li, B, Mg, Al, Mn, Fe, Cd, Ba, Nd, U), performed on all 34 samples, employed a Thermo Scientific Element 2-XR MC-ICP-MS and followed methods published in Fowell et al. (2016). Prior to $\delta^{11}B$ analyses, boron was isolated from the carbonate matrix of 10 samples by ion-exchange chromatography using custom made 20 µl Teflon columns filled with Amberlite IRA743 resin following Foster (2008) and Fowell et al. (2018). Boron isotope ratios were then measured on a Thermo Scientific Neptune MC-ICP-MS with mass bias correction by sample-

standard bracketing with NIST SRM951 following Foster et al. (2013). Uncertainty in bulk $\delta^{11}B$ was determined following Rae et al. (2011), based on the long-term reproducibility of the JCp-1 reference material (Okai et al., 2002), and was on average ±0.25 ‰ (2SD). The $\delta^{11}B$ of the JCp-1 used in this study was 24.14 ‰, consistent with both the long term results from JCp-1 analysis in this laboratory and with results from other laboratories (24.25±0.22; Gutjahr et al., 2020). For trace element ratios, the analytical precision is 5 % determined by the reproducibility of several in house standards (Henehan et al., 2015).

The study also adopts the novel use of LA-MC-ICP-MS to measure skeletal $\delta^{11}B$ (Thil et al., 2016; Sadekov et al., 2019; Standish et al., 2019). For this method, the coral slice was analyzed by a Thermo Scientific Neptune Plus MC-ICP-MS equipped with nine Faraday Cup detectors and a central ion counter coupled to a TwoVol2 cell of an Elemental Scientific Lasers NWR193 excimer laser ablation system at the University of Southampton, following a peak hopping approach that uses the $^{11}B/^{40}ArCa^{4+}$ to correct for matrix interferences from scattered Ca ions (Standish et al. 2019). Data were collected using integrations of 2.194 s and idle times of 2 s, and thus each data cycle was collected over a period of 8.388 s. Accuracy and external reproducibility is demonstrated by repeat analyses of the in-house reference material PS69/318–1, a cold water calcitic scleraxonian octocoral, which, over the course of this study, gave a mean value of 13.70±0.74 ‰ (all errors herein are 2SD). This is consistent with a solution MC-ICP-MS measurement of 13.83±0.29 ‰ (Standish et al. 2019). Six laser ablation transects (L1–L6) were placed approximately 280–500 μm from the micro-milling transect (LAA-1, Fig. 2b). The LA transects themselves were spaced 280–420 μm apart, approximately parallel to each other. Four additional laser ablation transects each of 1 cm length were placed perpendicular to the coral growth axis (HL1–HL4) around 2 cm from LAA-1 (LAA-2, Fig. 2b) aiming to quantify the small-scale variability evident in LA-MC-ICP-MS derived $\delta^{11}B$ of approximately similar-aged $CaCO_3$.

For all laser ablation analyses, a spot diameter of 140 μm was used, sampling at a tracking speed of 5 μm/s, a repetition rate of 12 Hz, and energy density (power) of 6 J cm^{-2}. With a total cycle time of ~8.4 seconds, one $\delta^{11}B$ data cycle corresponds to sample ablated over a distance of 182 μm along the LA transect. This translates into approximately 3.7 days of calcification. Along each LA transect, the distance between the centre points of ablated areas corresponding to

consecutive data cycles is ~40 μm, which translates into a sampling resolution of on average 0.8 days of calcification. However, subsequent smoothing of the data and averaging due to spot size reduces the effective resolution. Furthermore, the reproducibility of single LA data cycles is ±2.44 ‰ (2SD), based on analyses of the in-house reference material PS69/318–1, reducing our ability to resolve fine-temporal scale variability in $\delta^{11}B$.

The effect of an H_2O_2 treatment to oxidize any coral-organic material was explored for LA-MC-ICP-MS $\delta^{11}B$ by soaking the coral slice in 400 ml of 20% H_2O_2 solution for 24 hours after 3 (L1–L3) of the 6 laser ablation transects had been measured (LAA-1). All transects in LAA-2 were measured after H_2O_2 treatment.

Calculation of pH_{cf} from $\delta^{11}B$ followed Foster and Rae (2016) using the isotopic fractionation constant from Klochko et al. (2006). For pH_{cf} calculation, the value of the equilibrium constant for the dissociation of boric acid (pK^*_B) was determined using daily averages of temperature and salinity recorded by the CTD logger. Calculation of carbonate parameters from B/Ca followed DeCarlo et al. (2018) using the partition coefficient from McCulloch et al. (2018). Calculation of seawater carbonate parameters was performed using the R-package seacarb (Gattuso et al., 2019). Time series analysis of geochemical data was conducted in R (R Core Team, 2019) and Past (Hammer et al., 2001).

2.5 Numerical Modelling

Calcifying fluid pH upregulation of *Porites* sp. colonies growing on Cecile Peninsula reef flat was simulated using a numerical model described in Guo (2019). This model simulates the effects of three key processes involved in coral pH_{cf} upregulation, including enzymatic proton pumping (P), carbon influx (C), and the exchange of calcifying fluid with external seawater (E), and predicts pH_{cf} based on ambient seawater carbonate chemistry, temperature, and coral P/E ratio. The model was optimized by determining the average P/E ratio for the *Porites* sp. colony analyzed, based on the pH_{cf} data derived from our 10 bulk $\delta^{11}B$ measurements where a sample represents on average 11 days of calcification, as well as seawater carbonate chemistry parameters and temperature data averaged over equivalent time periods. Specifically, seawater carbonate chemistry parameters, such as dissolved inorganic carbon (DIC_{sw}) or Ω_{sw}, were estimated from SeaFET pH-sensor measurements of pH_{sw}, CTD recordings of temperature and salinity, and average TA_{sw} determined from reef flat seawater samples collected in September

2017 and May 2018, during day and night (Table S1). In the time interval when no SeaFET pH-sensor data were available, average values of seawater carbonate chemistry were used for optimizing the coral P/E ratio.

The optimized coral P/E value was then combined with high resolution (30 minute) recordings of pH_{sw} and temperature, as well as similarly resolved estimates of other seawater carbonate chemistry parameters to predict pH_{cf} upregulation on a diurnal scale. Specifically, DIC_{sw} and Ω_{sw} were estimated from 30 minutes measurements of pH_{sw}, temperature, salinity, and average TA_{sw} from day and night measurements in September 2017 and May 2018 on Cecile Peninsula reef flat (Table S1), as it was not possible to measure other carbonate system parameters with the same resolution as pH_{sw}. Sensitivity tests of model predictions in pH_{cf} to changes in TA_{sw} resulted in a sensitivity of -0.010±0.001 pH units per 100 μmol kg^{-1} increase in TA_{sw}. Thus, the small variability in TA_{sw} observed at the study site has no substantial effect on model predictions in pH_{cf}. For example, TA_{sw} varied by 43±143 μmol kg^{-1} between September 2017 and May 2018, while the mean diurnal range in TA_{sw} recorded was 49±65 μmol kg^{-1} consistent with the diurnal range in TA_{sw} reported previously at similar water depths, e.g., 43±39 μmol kg^{-1} (Zhang et al., 2013), 23±7 μmol kg^{-1}, and 71±23 μmol kg^{-1} (Lantz et al., 2014).

The physiological processes simulated in the model operate over a scale of seconds and thus the model is well capable of simulating diurnal variations in pH_{cf}. Note, however, that the model P/E ratio is optimized based on seasonal variations in pH_{sw} and temperature, and this is assumed constant throughout the model simulation. Some culturing experiments under constant pH_{sw} and temperature conditions showed that pH_{cf} is reduced in the absence of light, which is likely related to the light dependent photosynthetic activity of the zooxanthellae (Al-Horani et al., 2002; Venn et al., 2011; Sevilgen et al., 2019). Such physiological processes that occur at the diurnal scale and are largely independent of seawater conditions are not included in the model due to the assumption of constant model parameters across different time scales.

3 Results

3.1 Environmental Monitoring

Field measurements of pH_{sw} showed that at Cecile Peninsula reef flat average pH_{sw} is relatively stable throughout the year with slightly lower values in spring 2018 than during spring and

summer 2017 (Fig. 3c). During the first period of pH_{sw} measurements (14th May – 6th September 2017) average pH_{sw} was 7.99±0.14 and during the second period (9th March – 25th May 2018) average pH_{sw} was 7.96±0.20. However, a relatively large diurnal pH-cycle exists on the reef flat, with pH_{sw} ranging up to 8.37±0.01 during the day with a minimum value of 7.65±0.01 during the night (both measured on 4th April 2018, Fig. 3c and 4a) and a mean diurnal pH_{sw} range (ΔpH_{sw}) of 0.29±0.24 pH units.

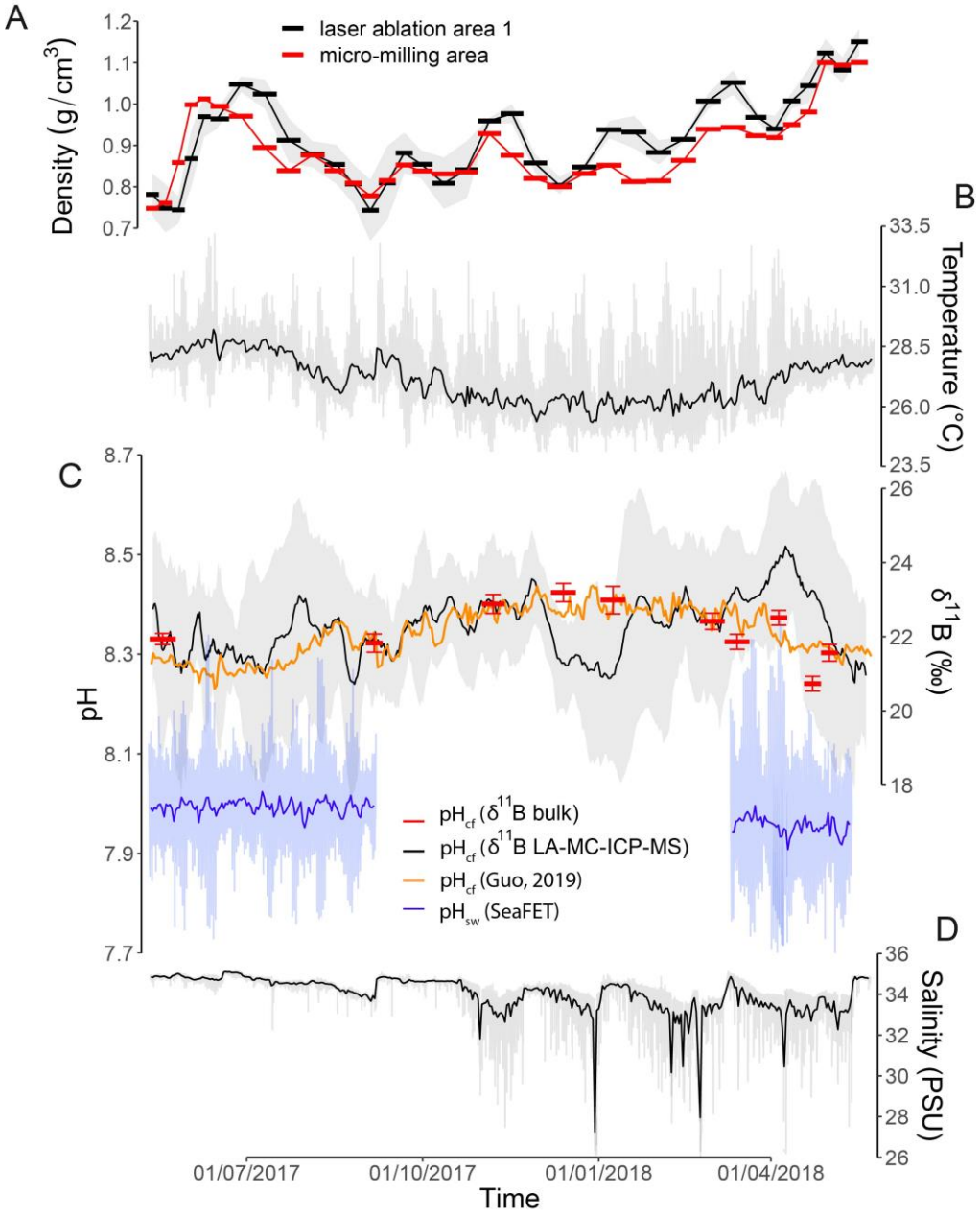

Figure 3. Skeletal density derived from X-ray densitometry (a), daily averaged seawater temperature from CTD logger (b), pH_{cf} reconstructed from $\delta^{11}B$ (LA-MC-ICP-MS plotted as an 8 point running mean, black) and modelled following Guo (2019, orange), pH_{sw} recorded by SeaFET pH-sensor (c) with daily averages (dark blue) and measured with a 30 min resolution (light blue), as well as daily averaged seawater salinity (d), grey lines in plot of temperature and salinity are 30 min measurements, and the grey area in $\delta^{11}B$ indicates standard deviation.

257

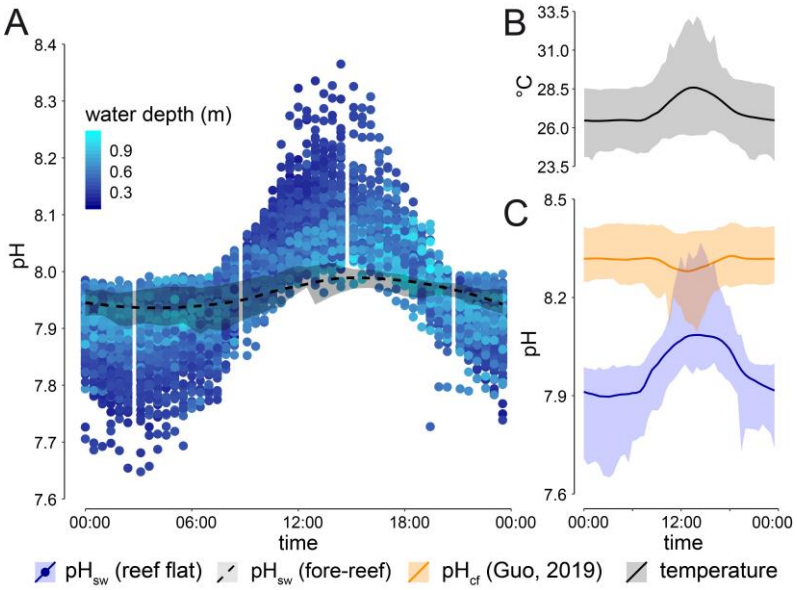

Figure 4. Diurnal pH_{sw}-cycle and water depth relative to the position of CTD logger. The average pH_{sw} measured on the fore-reef is indicated as a dashed line with maximum and minimum pH_{sw} measured at a given time contoured as greyed area (a). Diurnal temperature cycle with greyed area indicating minimum and maximum values recorded at a specific time (b). Diurnal cycle of pH_{cf} (orange) from numerical modelling and pH_{sw} (blue) as recoded by SeaFET pH-sensor. Transparent areas indicate the minimum and maximum values recorded at a given time (c).

258 Average pH_{sw} on the fore-reef recorded over the 9-day period was 7.96±0.05, thus similar to
259 average reef flat pH recorded over the one-year period, and very close to average reef flat pH of

7.94±0.17 recorded during the 9 days of sampling before moving the SeaFET pH-sensor to the fore-reef. However, the diurnal pH_{sw} range was substantially lower on the fore-reef with ΔpH_{sw} = 0.07±0.05 over the 9 days sampling interval (Fig. 4a). The highest pH_{sw} recorded on the fore-reef was 8.02±0.01 and the lowest was 7.89±0.01. Day and night measurements of TA_{sw}, that showed only little variability, pH_{sw} temperature and salinity on the reef flat and fore-reef were used to calculate other seawater carbonate parameters (Table S1). On the reef flat, DIC_{sw} and Ω_{sw} revealed a similar diurnal divergence from daily average as pH_{sw}, but notably, daily averages on the reef flat for these other carbonate system parameters were also similar to values on the fore-reef.

Reef flat CTD seawater temperature measurements revealed an annual average of 27.1±2.6 °C and a clear seasonal pattern with a maximum daily average value of 29.2±3.2 °C recorded during summer (14th June 2017) and a minimum of 25.3±1.0 °C during winter (28th December 2017, Fig. 3b). Mean temperature on the fore-reef between the 28th May and 5th June 2018 was 27.7±0.3 °C, comparable to that recorded on the reef flat between the 3rd and 11th of May (27.8±1.17 °C). The diurnal temperature range observed on the fore-reef was 0.3±0.2°C, substantially lower than that on the reef flat which exhibited a diurnal temperature range of 1.7±1.2°C between the 3rd and 11th May 2018.

On the reef flat, average annual salinity was 34.0±2.3 PSU. During strong rainfall events in winter and spring, average daily salinity decreased to 27.3±1.1 PSU (30th December 2017), indicating the formation of a temporary low-salinity layer (Fig. 4d). Mean salinity recorded on the fore-reef over the 9 days sampling period was 34.9±0.08 PSU that is only slightly higher than that measured on the reef flat between the 3rd to 11th of May on the reef flat (34.8±2.0 PSU).

3.2 Geochemical Analysis and X-ray Densitometry

It is known from previous studies that due to low rainfall rates on Kiritimati Island coral $\delta^{18}O$ closely follows SST with little effect of seawater salinity (McGregor et al. 2011). Thus, the alignment of coral $\delta^{18}O$ with seawater temperatures recorded by the CTD logger enabled the construction of an age-depth model for the annual growth band (Fig. S5).

Values of $\delta^{11}B$ measured with conventional dissolution (bulk analysis) remained relatively stable along the annual growth band with an average of 22.09±1.46 ‰ and a variance of 0.53 ‰ (Fig. 3c). The mean of the 6 laser ablation transects of LAA-1 revealed a similar average $\delta^{11}B$ of 22.20±1.64 ‰, but with large variation around this value from 16.02 ‰ to 27.57 ‰ and a variance of 2.16 ‰ (Fig. 3c). The good agreement in average $\delta^{11}B$ between both methods validates the accuracy of LA-MC-ICP-MS measurements of $\delta^{11}B$. The apparently higher $\delta^{11}B$ from LA-MC-ICP-MS in the outermost 5 mm of the annual band might result from tissue layer organic matter residues which are also seen to reduce $\delta^{13}C$ and U/Ca, as well as increase Cd/Ca in this area (Fig. S2). However, the treatment of samples with H_2O_2 to remove organic constituents did not seem to affect the results (Fig. S3). Laser ablation measurements before the sample was treated with H_2O_2 (transect L1, L2, and L3) resulted in a mean $\delta^{11}B$ of 22.01±2.16 ‰ with a variance of 1.59 ‰. Similarly, measurements after H_2O_2 treatment (transect L4, L5, and L6) revealed a mean $\delta^{11}B$ of 22.39±2.52 ‰ with a variance of 2.45 ‰.

Results of LA-MC-ICP-MS $\delta^{11}B$ analysis along the four transects perpendicular to the coral's growth axis (LAA-2, Fig. 2b) reflects the $\delta^{11}B$ variability in $CaCO_3$ that was precipitated nearly synchronously (Fig. S4). Therefore, the observed variabilities in $\delta^{11}B$ along these transects are not simply due to variations in ambient seawater conditions, but likely result from sampling different components of the coral skeleton macrostructure with variable $\delta^{11}B$. Results show that the variance observed in $\delta^{11}B$ transects of LAA-2 was around 50% lower (HL1: σ^2 = 1.92 ‰, HL2: σ^2 = 2.67 ‰, HL3: σ^2 = 1.18 ‰, HL4: σ^2 = 1.47 ‰) than in transects from LAA-1 (L1: σ^2 = 2.13 ‰, L2: σ^2 = 3.02 ‰, L3: σ^2 = 3.76 ‰, L4: σ^2 = 4.5 ‰, L5: σ^2 = 3.87 ‰, L6:σ^2 = 2.42 ‰). This suggests that approximately half of the variability in each of the $\delta^{11}B$ transects from LAA-1 results from sampling different components of the coral skeleton macrostructure. Similar $\delta^{11}B$ heterogeneities have been found in other coral $\delta^{11}B$ LA-MC-ICP-MS studies (Chalk et al., 2021) and are likely linked to spatial variations of pH_{cf} in the coral skeleton as shown in studies using pH-sensitive dyes or microelectrodes (Venn et al. 2011, Cai et al. 2016, Sevilgen et al. 2019). These macrostructural heterogeneities in skeletal $\delta^{11}B$ may also explain the short-term differences between bulk and LA-MC-ICP-MS derived $\delta^{11}B$ in some intervals (Fig. 3c), as well as some of the differences between individual LA $\delta^{11}B$ transects L1–6. The remaining variability within and across the $\delta^{11}B$ transects can, at least in part, be attributed to the relatively low precision of the LA-MC-ICP-MS measurements here compared to solution-based approaches.

Skeletal density variations measured for micro-milling area and LAA-1 (Fig. 3a) showed a high level of agreement ($r^2 = 0.72$, $p < 0.01$, $n = 36$). Estimated skeletal density was in the lower range of previously reported values for *Porites* (Tanzil et al. 2016, Tortolero-Langarica et al. 2016, Mollica et al. 2018) with on average 0.89±0.19 g cm^{-3} (micro-milling area), 0.91±21 g cm^{-3} (LLA-1) respectively. The highest density values were measured at the edge of the annual band (1.15 g cm^{-3}) and another local maximum at 15.75 to 14.25 mm depth (1.00 g cm^{-3}). The lowest values were found at the base and of the annual band and at 12 mm depth (0.75 g/cm^{-3}).

3.3 Numerical Modelling

Theoretical modeling showed that the coral's physiological regulation of pH_{cf} is best represented by the interplay between enzymatic proton pumping (P) and the exchange of calcifying fluid with external seawater (E), i.e. a colony specific P/E ratio (Guo, 2019). Thus, the numerical model of pH_{cf} upregulation (Guo, 2019) was first optimized to determine the average P/E ratio specific to the *Porites* sp. specimen employed in this study (see section 2.5). With this optimized P/E ratio, this model successfully reproduced the pH_{cf} derived from bulk $\delta^{11}B$ measurements (Fig. 3c) and predicts only limited diurnal pH_{cf} variability (Fig. 4c). The model predicted a mean diurnal range in pH_{cf} of ΔpH_{cf} = 0.07±0.08 with a maximum ΔpH_{cf} of 0.21 (1st April 2018) and a minimum of 0.03 (21st July 2017). Notably, this is substantially lower than the diurnal range in ambient pH_{sw} of on average 0.29±0.24 pH units.

4 Discussion

4.1 Variability in Reef Flat Environmental Conditions

On a seasonal scale, variations of seawater temperature affect pH_{sw} through the temperature dependency of dissociation constants. However, only a weak correlation ($r^2 = 0.16$, $p < 0.01$, $n = 179$) between daily averages of pH_{sw} on the reef flat and seawater temperatures was found (Fig. 3b and c, Fig. S6a). Due to the failure of the SeaFET pH-sensor, it was not possible to analyze a full seasonal cycle and this limitation may be obscuring any correlations. On the other hand, seasonal temperature variations at Kiritimati Island were low (4 °C) and thus the effect of temperature is likely superseded by other environmental factors. Across the monitoring period that pH_{sw} was recorded, daily averages of pH_{sw} and salinity showed the highest degree of correlation ($r^2 = 0.56$, $p < 0.01$, $n = 179$, Fig. S6b). Heavy rainfall events in winter 2017/2018

and spring 2018 caused the formation of a low-salinity layer on the reef flat and this dilution of seawater by meteoric water explains the lower pH_{sw} values recorded during spring 2018 compared to spring and summer 2017 (0.04 pH units, Fig. 3c and d).

Agreement between daily averages of pH_{sw} measured with the SeaFET pH-sensor (Fig. 4a), and the other carbonate system parameters calculated from TA_{sw} and portable pH-meter measurements between the reef flat and fore-reef (Table S1), indicates that average seawater conditions on the reef flat are influenced by, and reflect, off reef conditions. However, the amplitude of the diurnal pH_{sw} and temperature cycles on the reef flat exceeded those on the fore-reef by half an order of magnitude (Fig. 4a), as reported previously in other reef systems (Cyronak et al., 2019). A number of studies have detailed that the balance between Net Ecosystem Productivity (NEP) and Net Ecosystem Calcification (NEC) drives the diurnal pH_{sw} cycle on the reef (Smith, 1973; Gattuso et al., 1993; DeCarlo et al., 2017). NEP describes the rates of photosynthesis and respiration that occur on the reef, whereby photosynthesis removes CO_2 from the seawater increasing pH_{sw}, and respiration releases CO_2 reducing pH_{sw} (Cyronak et al., 2018). NEC is controlled by the rate of calcification and dissolution whereby calcification releases CO_2 lowering pH_{sw} and dissolution consumes CO_2 increasing pH_{sw}. As photosynthesis dominates during the day, and respiration during the night, pH_{sw} oscillates diurnally (Fig. 3c and 4a). During days with elevated solar irradiance photosynthesis is stimulated and the maximum of the diurnal pH_{sw} cycle tends towards higher values than on days with cloud cover. Elevated solar irradiance also leads to elevated seawater temperatures. A significant positive correlation (r^2 = 0.40, $p < 0.01$, n = 179) between average pH_{sw} and temperature, measured between 12 pm and 4 pm when the diurnal pH_{sw} cycle peaks (Fig. S7), confirms this dependency for the reef flat (Fig. S7a). However, the main driver of the diurnal pH_{sw} cycle's magnitude on the reef flat appears to be the tidal cycle (Shaw et al., 2012; Chan & Eggins, 2017). The water level on the reef flat determines the seawater residence time and thus how much seawater with low (night) or high (day) pH_{sw} levels remains on the reef flat or is removed in exchange with seawater off reef with more moderate pH_{sw}. If low tide occurs during the maximum and minimum of the diurnal pH_{sw} cycle, which is at approximately 12 pm to 4 pm, and 2 am respectively, the products of NEP and NEC accumulate in a smaller volume of water. This amplifies the diurnal pH_{sw} range by further increasing pH_{sw} during the day and lowering pH_{sw} during the night (Fig. 4a). This is evident by a negative correlation between averaged pH_{sw} and water depth during the day time (12 pm to 4

pm) in the time interval 14th May – 6th September 2017 ($r^2 = 0.47$, $p < 0.01$, $n = 119$), as well as in the in the time interval 9th March – 25th May 2018 ($r^2 = 0.53$, $p < 0.01$, $n = 63$), and the positive correlation at night time (2 am) in the time interval 14th May – 6th September 2017 ($r^2 = 0.39$ $p < 0.01$, $n = 119$), and in the time interval 9th March – 25th May 2018 ($r^2 = 0.51$, $p < 0.01$, $n = 63$), respectively (Fig. S8). Finally, the influences of low water levels on pH_{sw} are most evident during spring tides and the smallest during neap tides. Hence, daily maxima and minima values of pH_{sw} oscillate with a periodicity of 15 days that is equivalent to the average periodicity of the occurrence of spring tides or half a synodic month (Fig. 3c, Fig. 5a, Fig. S9a–d). Elevated day time (12 pm to 4 pm) seawater temperatures occur with a similar periodicity as smaller volumes of water during low spring tides warm up quicker (Fig. 3b, Fig. 5b, Fig. S9e). However, the effect of spring and neap tides is less significant in time series of seawater temperatures than of pH_{sw}.

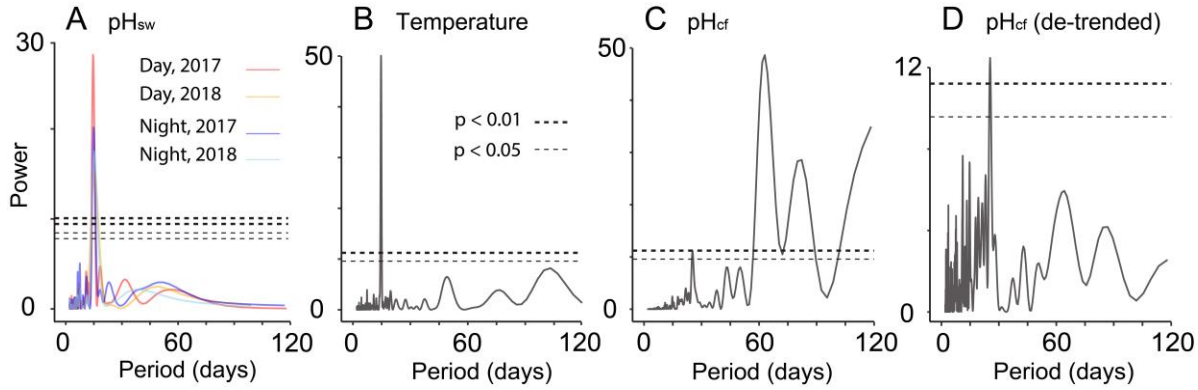

Figure 5. The amplitude of the reef flat pH_{sw} and temperature cycle oscillate with a 15 days periodicity: Results of spectral analysis of day time (12–4 pm) and night time (2 am) pH_{sw} (a) and day time (12–4 pm) seawater temperature (b). No similar periodicity was found in time series of LA-MC-ICP-MS $\delta^{11}B$ derived pH_{cf} (c) or the similar de-trended (differenced) time series (d). Confidence lines are indicated as thick ($p < 0.01$) and thin ($p < 0.05$) dashed lines whereas in (a) confidence lines of day and night 2017 overlap at power = 10.08 ($p < 0.01$) and power = 8.44 ($p < 0.05$), as well as the confidence lines of day and night 2018 at power = 9.44 ($p < 0.01$) and power = 7.81 ($p < 0.05$).

It can be concluded that on a seasonal scale, daily averaged pH_{sw} at Cecile Peninsula reef flat on Kiritimati Island appears to remain relatively stable, likely following off reef trends, with the

long-term pH_{sw} variability being caused by large rainfall events diluting the seawater and causing a reduction in pH_{sw}. On the diurnal cycle, the occurrence of maxima and minima $pH_{sw,}$ and maxima of seawater temperatures followed the 15 days spring-neap tidal cycle and associated variations of sea level.

4.2 Variability in pH_{cf} Upregulation

In the time intervals when both pH_{sw} and pH_{cf} data are available, the coral upregulated pH_{cf} on average by 0.33 pH units for bulk $\delta^{11}B$ and 0.37 pH units for LA-MC-ICP-MS $\delta^{11}B$, respectively (Fig. 3c). This is similar to the level of pH_{cf} upregulation reported for *Porites* by McCulloch et al. (2017) and in the same range as other studies (Hönisch et al., 2004; Krief et al., 2010; Georgiou et al., 2015; Wall et al., 2016). In addition to pH_{cf}, estimates based on B/Ca ratios suggest calcifying fluid dissolved inorganic carbon (DIC_{cf}) was elevated by a factor of 2.4, calcifying fluid total alkalinity (TA_{cf}) by 2.5, and calcifying fluid aragonite saturation state (Ω_{cf}) by 4.2 compared to ambient seawater conditions on the reef flat (Fig. S10, Table S1). These results are also in the range reported in a previous study (Comeau et al., 2017).

On a seasonal scale, $\delta^{11}B$ derived coral pH_{cf} did not show any significant correlation with variations of pH_{sw} as recorded by the SeaFET pH-sensor (Fig. 6a). Indeed, in the time interval 9th March – 25th May 2018 where pH_{sw} values were slightly reduced (-0.04 pH units) due to the formation of a low-salinity layer on the reef flat, laser ablation $\delta^{11}B$ derived pH_{cf} remained slightly elevated (+0.09 pH units, Fig. 3c). Seawater temperature appeared to be the main driver of observed pH_{cf} variations with $r^2 = 0.58$ ($p < 0.01$, $n = 10$) between pH_{cf} calculated from bulk $\delta^{11}B$ and seawater temperatures (Fig. 3b and c, Fig. 6b). A predominant control of ambient seawater temperatures on *Porites* pH_{cf} upregulation on a seasonal scale is in accordance with other recent studies (McCulloch et al., 2017; Ross et al., 2017; Guo, 2019), as well as those that revealed a limited sensitivity of *Porites* pH_{cf} upregulation to seasonal variations in pH_{sw} (Georgiou et al., 2015; Comeau et al., 2019).

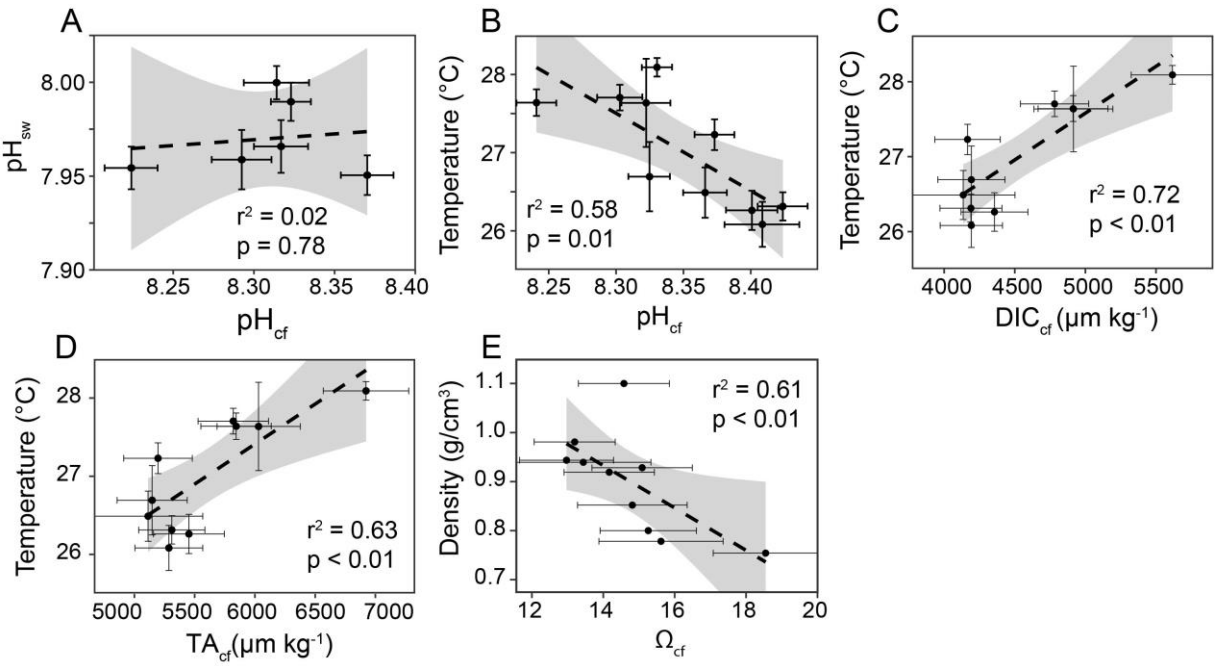

Figure 6: Controls on calcifying fluid carbonate chemistry parameters. Correlations between pH_{sw} and pH_{cf} (bulk $\delta^{11}B$, a), as well as between seawater temperature and calcifying fluid carbonate chemistry parameters, such as pH_{cf} (b), DIC_{cf} (c) and TA_{cf} (d) are shown. Furthermore, the correlation between Ω_{cf} and skeletal density is presented (e).

Corals calcify predominantly during the day as light stimulates calcification (Buchsbaum & Muscatine, 1971; Cohen et al., 2016). Potentially, highly resolved time series of $\delta^{11}B$ derived pH_{cf} could thus be biased towards day time pH_{cf} and consequently may record oscillations in day time pH_{cf}. However, no significant 15 days periodicity following the spring-neap tidal cycle as observed for day time pH_{sw} and temperature has been found in time series of LA-MC-ICP-MS $\delta^{11}B$ derived pH_{cf} (Fig. 5c and d, Fig. S9). This supports the numerical model results suggesting a limited diurnal variability in pH_{cf} despite the substantial diurnal variabilities in pH_{sw} (Fig. 4c) and temperature (Fig. 4b) observed on the reef flat. Furthermore, these findings are in accordance with previous studies that cultured corals under variable diurnal ranges in pH_{sw} and found similar levels in pH_{cf} upregulation across treatments (Cornwall et al., 2018), as well as no decline in calcification rates with increasing diurnal pH_{sw} variability (Enochs et al., 2018). In our model simulations, the competing effects of varying pH_{sw} and temperature on pH_{cf} upregulation (e.g. Guo 2019) result in a nearly constant pH_{cf} at the diurnal scale. However, as noted earlier,

diurnal physiological processes, such as light dependent variations in zooxanthellae photosynthetic activity, are not considered in our model and may still induce some diurnal variability in pH_{cf}. Of note, a significant periodicity of 25–26 days in the de-trended time series of LA-MC-ICP-MS $\delta^{11}B$ derived pH_{cf} (Fig. 5d) may relate to the accretion of dissepiments within the coral skeleton that follows the lunar cycle (DeCarlo & Cohen, 2017).

Besides pH_{cf}, other calcifying fluid carbonate system parameters calculated from bulk derived $\delta^{11}B$ and B/Ca also exhibit a seawater temperature dependency, such as DIC_{cf} ($r^2 = 0.72$, $p < 0.01$, $n = 10$, Fig. 6c) and TA_{cf} ($r^2 = 0.63$, $p < 0.01$, $n = 10$, Fig. 6d). Similarly, sub-annual variations in skeletal density suggest some positive relation with temperature, with lower density values in autumn and winter when seawater temperatures are low, and higher density in spring and summer under higher seawater temperatures (Fig. 3a and b), consistent with faster aragonite precipitation and thus skeletal densification at higher temperatures (Mollica et al., 2018; Guo et al., 2020). However, these sub-annual skeletal densities exhibited an apparent negative correlation with aragonite Ω_{cf} ($r^2 = 0.44$, $p = 0.04$, $n = 5$, Fig. 6e), different from the positive correlation between inter-annual skeletal density and Ω_{cf} observed in *Porites* collected from several Pacific reefs in Mollica et al. (2018). This difference likely reflects the interplay of multiple factors influencing coral skeletal density (e.g. extension rates, temperature, Ω_{cf}) on different time scales (Guo et al. 2020). Overall, our results support that coral calcification is affected by physiological modification of the calcifying fluid carbonate chemistry and that these modifications primarily follow variations in ambient seawater temperatures. However, while we have followed the DeCarlo et al. (2018) approach in converting B/Ca to $[CO_3^{2-}]$, it should also be noted that others have suggested there is a temperature dependency of boron incorporation into aragonite (Chen et al., 2015; Cai et al., 2016). This may be complicating the estimates of calcifying fluid carbonate system parameters we make here from B/Ca.

5 Conclusions

This study confirms that *Porites* pH_{cf} is upregulated compared to ambient pH_{sw} and that, on a season scale, seawater temperatures exert the primary control on pH_{cf} upregulation rather than pH_{sw} at our study location. Reduced reef flat pH_{sw} resulted from dilution by meteoric water occurring in response to periodic rainfall events, and was not reflected in time series of pH_{cf}. The

observed variations in pH_{cf} upregulation that follow ambient seawater temperatures are likely related to the temperature dependency of calcification rates. The application of a recent numerical model of pH_{cf} upregulation (Guo, 2019) and the novel usage of LA-MC-ICP-MS to determine skeletal $\delta^{11}B$ in high resolution (Standish et al., 2019) suggest that *Porites* also maintains pH_{cf} upregulation under large diurnal variations in reef flat pH_{sw} and temperature conditions, although, diurnally resolved measurements of pH_{cf} are needed to validate this finding. The observed diurnal pH_{sw} variability on Cecile Peninsula reef flat on Kiritimati Island was substantially higher than on the fore-reef, driven by ecological and tidal processes. In order to ensure calcification in such a dynamic pH_{sw} environment, *Porites* likely maintains upregulation of calcifying fluid carbonate chemistry parameters at seasonal and diurnal time scales.

Acknowledgments, Samples, and Data

The authors would like to thank the Royal Society Te Apārangi Marsden Fund New Zealand for funding this project (Project no. UOA1513, to P.K.), as well as the Investment in Science Fund and The Andrew W. Mellon Foundation Endowed Fund for Innovative Research at the Woods Hole Oceanographic Institution (to W.G.). We would also like to acknowledge Heather Goring-Harford, Megan Wilding, Bastian Hambach and J. Andy Milton from the University of Southampton, Emily Frost, Brendan Hall, Shane Cronin, Susan Owen and Catherine Hobbis from the University of Auckland, Taratau Kirata and Tataua from the Fishery Department of Kiritimati Island, Kim Currie and Judith Murdoch from the University of Otago, Andrew Lorrey and Christian Hyde from NIWA and the staff of the Mercy Radiology Auckland for their support during fieldwork, sample preparation and laboratory work.
Fieldwork was undertaken under Research Permit No. 010/16, provided by the Ministry of Environment, Lands and Agricultural Development, Government of Kiribati.

Data Availability Statement

The data used in this paper have been deposited in a general data repository. Data are available at https://auckland.figshare.com/articles/dataset/Knebel_2020_JGR_Oceans_/12774632 (doi: 10.17608/k6.auckland.12774632).

Conflict of Interest

The authors have no conflict of interest to declare.

References

Al-Horani, F. A., Al-Moghrabi, S. M., & de Beer, D. (2002). The mechanism of calcification and its relation to photosynthesis and respiration in the scleractinian coral Galaxea fascicularis. *Marine Biology, 142*(3), 419-426. doi:10.1007/s00227-002-0981-8

Bakker, D. C. E., Pfeil, B., Landa, C. S., Metzl, N., O'Brien, K. M., Olsen, A., . . . Xu, S. (2016). A multi-decade record of high-quality fCO2 data in version 3 of the Surface Ocean CO2 Atlas (SOCAT). *Earth System Science Data, 8*(2), 383-413. doi:10.5194/essd-8-383-2016

Bates, N. R., Amat, A., & Andersson, A. J. (2010). Feedbacks and responses of coral calcification on the Bermuda reef system to seasonal changes in biological processes and ocean acidification. *Biogeosciences, 7*(8), 2509-2530. doi:10.5194/bg-7-2509-2010

Bindoff, N. L., Cheung, W. W. L., Kairo, J. G., Arístegui, J., Guinder, V. A., Hallberg, R., . . . Williamson, P. (2019). Changing Ocean, Marine Ecosystems, and Dependent Communities. In H. -. Pörtner, D. C. Roberts, V. Masson-Delmotte, P. Zhai, M. Tignor, E. Poloczanska, . . . N. M. Weyer (Eds.), *IPCC Special Report on the Ocean and Cryosphere in a Changing Climate* In press.

Buchsbaum, V. P., & Muscatine, L. (1971). Role of Symbiotic Algae (Zooxanthellae) in Coral Calcification. *Biological Bulletin, 141*(2), 350-363. doi:10.2307/1540123

Cai, W., Ma, Y., Hopkinson, B. M., Grottoli, A. G., Warner, M. E., Ding, Q., . . . Wang, Y. (2016). Microelectrode characterization of coral daytime interior pH and carbonate chemistry. *Nature Communications, 7*(1), 11144. doi:10.1038/ncomms11144

Carricart-Ganivet, J. P., & Barnes, D. J. (2007). Densitometry from digitized images of X-radiographs: Methodology for measurement of coral skeletal density. *Journal of Experimental Marine Biology and Ecology, 344*(1), 67-72. doi:10.1016/j.jembe.2006.12.018

Chalk, T. B., Standish, C. D., Angelo, C. D., Castillo, K. D., Milton, J. A., & Foster, G. L. (2021). Mapping coral calcification strategies from in situ boron isotope and trace element measurements of the tropical coral Siderastrea siderea. *Scientific Reports, 11*(472) Retrieved from https://doi.org/10.1038/s41598-020-78778-1

Chan, W., & Eggins, S. (2017). Calcification responses to diurnal variation in seawater carbonate chemistry by the coral Acropora formosa. *Coral Reefs, 36*(3), 763-772. doi:10.1007/s00338-017-1567-8

Chen, T., Yu, K., Zhao, J., Yan, H., Song, Y., Feng, Y., & Chen, T. (2015). Testing coral paleothermometers (B/Ca, Mg/Ca, Sr/Ca, U/Ca and δ 18O) under impacts of large riverine runoff. *Acta Oceanologica Sinica, 34*(8), 20-26. doi:10.1007/s13131-015-0705-9

Cobb, K. M., Cheng, H., Edwards, R. L., & Charles, C. D. (2003). El Niño/Southern Oscillation and tropical Pacific climate during the last millennium. *Nature, 424*(6946), 271-276. doi:10.1038/nature01779

Cohen, I., Dubinsky, Z., & Erez, J. (2016). Light Enhanced Calcification in Hermatypic Corals: New Insights from Light Spectral Responses. *Frontiers in Marine Science, 2* doi:10.3389/fmars.2015.00122

Comeau, S., Cornwall, C. E., & McCulloch, M. T. (2017). Decoupling between the response of coral calcifying fluid pH and calcification to ocean acidification. *Scientific Reports (Nature Publisher Group), 7*(1), 7573. doi:10.1038/s41598-017-08003-z

Comeau, S., Cornwall, C. E., DeCarlo, T. M., Doo, S. S., Carpenter, R. C., & McCulloch, M. T. (2019). Resistance to ocean acidification in coral reef taxa is not gained by acclimatization. *Nature Climate Change, 9*(6), 477-483. doi:10.1038/s41558-019-0486-9

Comeau, S., Cornwall, C. E., DeCarlo, T. M., Krieger, E., & McCulloch, M. T. (2018). Similar controls on calcification under ocean acidification across unrelated coral reef taxa. *Global Change Biology, 24*(10), 4857-4868. doi:10.1111/gcb.14379

Constantz, B. R. (1986). Coral Skeleton Construction: A Physiochemically Dominated Process. *Palaios, 1*(2), 152-157. doi:10.2307/3514508

Cornwall, C. E., Comeau, S., DeCarlo, T. M., Moore, B., D'Alexis, Q., & McCulloch, M. T. (2018). Resistance of corals and coralline algae to ocean acidification: physiological control of calcification under natural pH variability. *Proceedings. Biological Sciences, 285*(1884), 20181168. doi:10.1098/rspb.2018.1168

Cyronak, T., Andersson, A. J., Langdon, C., Albright, R., Bates, N. R., Caldeira, K., . . . Yamamoto, S. (2018). Taking the metabolic pulse of the world's coral reefs. *PloS One, 13*(1), e0190872. doi:10.1371/journal.pone.0190872

Cyronak, T., Schulz, K. G., & Jokiel, P. L. (2016). The Omega myth: what really drives lower calcification rates in an acidifying ocean. *ICES Journal of Marine Science, 73*(3), 558-562. doi:10.1093/icesjms/fsv075

542 Cyronak, T., Takeshita, Y., Courtney, T. A., DeCarlo, E. H., Eyre, B. D., Kline, D. I., . . . Andersson, A. J. (2019).
543 Diel temperature and pH variability scale with depth across diverse coral reef habitats. *Limnology and*
544 *Oceanography Letters*, *5*(2) doi:10.1002/lol2.10129
545 DeCarlo, T. M., Cohen, A. L., Wong, G. T. F., Shiah, F., Lentz, S. J., Davis, K. A., . . . Lohmann, P. (2017).
546 Community production modulates coral reef pH and the sensitivity of ecosystem calcification to ocean
547 acidification. *Journal of Geophysical Research: Oceans*, *122*(1), 745-761. doi:10.1002/2016JC012326
548 DeCarlo, T. M., Holcomb, M., & McCulloch, M. T. (2018). Reviews and syntheses: revisiting the boron systematics
549 of aragonite and their application to coral calcification. *Biogeosciences, 15*, 2819-2834. doi:10.5194/bg-15-
550 2819-2018
551 DeCarlo, T., & Cohen, A. (2017). Dissepiments, density bands and signatures of thermal stress in Porites skeletons.
552 *Coral Reefs*, *36*(3), 749-761. doi:10.1007/s00338-017-1566-9
553 DeCarlo, T., Ross, C., & McCulloch, M. (2019). Diurnal cycles of coral calcifying fluid aragonite saturation state.
554 *Marine Biology, 166*(3), 1-6. doi:10.1007/s00227-019-3468-6
555 Dickson, A. G., Sabine, C. L., & Christian, J. R. (2007). *Guide to Best Practices for Ocean CO2 Measurement.* (
556 No. 3).PICES Special Publication.
557 D'Olivo, J. P., Ellwood, G., DeCarlo, T. M., & McCulloch, M. T. (2019). Deconvolving the long-term impacts of
558 ocean acidification and warming on coral biomineralisation. *Earth and Planetary Science Letters*, *526*,
559 115785. doi:10.1016/j.epsl.2019.115785
560 Doney, S. C., Busch, D. S., Cooley, S. R., & Kroeker, K. J. (2020). The Impacts of Ocean Acidification on Marine
561 Ecosystems and Reliant Human Communities. *Annual Review of Environment and Resources*, *45*(1), 83-112.
562 doi:10.1146/annurev-environ-012320-083019
563 Duarte, C. M., Hendriks, I. E., Moore, T. S., Olsen, Y. S., Steckbauer, A., Ramajo, L., . . . McCulloch, M. (2013). Is
564 Ocean Acidification an Open-Ocean Syndrome? Understanding Anthropogenic Impacts on Seawater pH.
565 *Estuaries and Coasts*, *36*, 221–236. doi:10.1007/s12237-013-9594-3
566 Enochs, I. C., Manzello, D. P., Jones, P. J., Aguilar, C., Cohen, K., Valentino, L., . . . Lirman, D. (2018). The
567 influence of diel carbonate chemistry fluctuations on the calcification rate of Acropora cervicornis under
568 present day and future acidification conditions. *Journal of Experimental Marine Biology and Ecology, 506*,
569 135-143. doi:10.1016/j.jembe.2018.06.007

570 Foster, G. (2008). Seawater pH, pCO2 and CO2−3] variations in the Caribbean Sea over the last 130 kyr: A boron
571 isotope and B/Ca study of planktic foraminifera. *Earth and Planetary Science Letters, 271*, 254-266.
572 doi:10.1016/j.epsl.2008.04.015
573 Foster, G. L., Hönisch, B., Paris, G., Dwyer, G. S., Rae, J. W. B., Elliott, T., . . . Vengosh, A. (2013). Interlaboratory
574 comparison of boron isotope analyses of boric acid, seawater and marine CaCO3 by MC-ICPMS and NTIMS.
575 *Chemical Geology, 358*, 1-14. doi:10.1016/j.chemgeo.2013.08.027
576 Foster, G. L., & Rae, J. W. B. (2016). Reconstructing Ocean pH with Boron Isotopes in Foraminifera. *Annual*
577 *Review of Earth and Planetary Sciences, 44*(1), 207-237. doi:10.1146/annurev-earth-060115-012226
578 Fowell, S. E., Foster, G. L., Ries, J. B., Castillo, K. D., Vega, E., Tyrrell, T., . . . Chalk, T. B. (2018). Historical
579 Trends in pH and Carbonate Biogeochemistry on the Belize Mesoamerican Barrier Reef System. *Geophysical*
580 *Research Letters, 45*(7), 3228-3237. doi:10.1002/2017GL076496
581 Fowell, S. E., Sandford, K., Stewart, J. A., Castillo, K. D., Ries, J. B., & Foster, G. L. (2016). Intrareef variations in
582 Li/Mg and Sr/Ca sea surface temperature proxies in the Caribbean reef-building coral Siderastrea siderea.
583 *Paleoceanography, 31*(10), 1315-1329. doi:10.1002/2016PA002968
584 Friedlingstein, P., Jones, M. W., O'Sullivan, M., Anew, R. M., Hauck, J., Peters, G. P., . . . Zaehle, S. (2019). Global
585 carbon budget 2019. *Earth System Science Data, 11*(4), 1783. Retrieved from
586 https://www.narcis.nl/publication/RecordID/oai:dspace.library.uu.nl:1874%2F388384
587 Gattuso, J. -., Pichon, M., Delesalle., B., & Frankignoulle, M. (1993). Community metabolism and air-sea CO2
588 fluxes in a coral reef ecosystem (Moorea, French Polynesia). *Marine Ecology Progress Series, 96*(3), 259-267.
589 doi:10.3354/meps096259
590 Gattuso, J. P., Epitalon, J., Lavigne, H., & Orr, J. (2019). *seacarb: Seawater Carbonate Chemistry. R package*
591 Gattuso, J., Allemand, D., & Frankignoulle, M. (1999). Photosynthesis and Calcification at Cellular, Organismal and
592 Community Levels in Coral Reefs: A Review on Interactions and Control by Carbonate Chemistry. *American*
593 *Zoologist, 39*(1), 160-183. doi:10.1093/icb/39.1.160
594 Georgiou, L., Falter, J., Trotter, J., Kline, D. I., Holcomb, M., Dove, S. G., . . . McCulloch, M. (2015). pH
595 homeostasis during coral calcification in a free ocean CO2enrichment (FOCE) experiment, Heron Island reef
596 flat, Great Barrier Reef. *Proceedings of the National Academy of Sciences, 112*(43), 13219-13224.
597 doi:10.1073/pnas.1505586112

598 Guo, W. (2019). Seawater temperature and buffering capacity modulate coral calcifying pH. *Scientific Reports*, *9*(1),
599 1-13. doi:10.1038/s41598-018-36817-y
600 Guo, W., Bokade, R., Cohen, A. L., Mollica, N. R., Leung, M., & Brainard, R. E. (2020). Ocean Acidification has
601 Impacted Coral Growth on the Great Barrier Reef. *Geophysical Research Letters, 47*(19)
602 doi:10.1029/2019GL086761
603 Gutjahr, M., Bordier, L., Douville, E., Farmer, J., Foster, G. L., Hathorne, E. C., . . . You, C. (2020). Sub-permil
604 interlaboratory consistency for solution-based boron isotope analyses on marine carbonates. *Geostand Geoanal*
605 *Res.*, Retrieved from http://hdl.handle.net/10023/20982
606 Hammer, Ø, Harper, D. A. T., & Ryan, P. D. (2001). *PAST: Paleontological statistics software package for*
607 *education and data analysis*. Palaeontologia Electronica 4(1): 9pp:
608 Henehan, M. J., Foster, G. L., Rae, J. W. B., Prentice, K. C., Erez, J., Bostock, H. C., . . . Wilson, P. A. (2015).
609 Evaluating the utility of B/Ca ratios in planktic foraminifera as a proxy for the carbonate system: A case study
610 of Globigerinoides ruber. *Geochemistry, Geophysics, Geosystems, 16*(4), 1052-1069.
611 doi:10.1002/2014GC005514
612 Hönisch, B., Hemming, N. G., Grottoli, A. G., Amat, A., Hanson, G. N., & Bijma, J. (2004). Assessing scleractinian
613 corals as recorders for paleo-pH: Empirical calibration and vital effects. *Geochimica Et Cosmochimica Acta,*
614 *68*(18), 3675-3685. doi:10.1016/j.gca.2004.03.002
615 Kench, P. S., McLean, R. F., Owen, S. D., Ryan, E., Morgan, K. M., Ke, L., . . . Roy, K. (2019). Climate-forced sea-
616 level lowstands in the Indian Ocean during the last two millennia. *Nature Geosecience*, doi:10.1038/s41561-
617 019-0503-7
618 Klochko, K., Kaufman, A. J., Yao, W., Byrne, R. H., & Tossell, J. A. (2006). Experimental measurement of boron
619 isotope fractionation in seawater. *Earth and Planetary Science Letters, 248*(1), 276-285.
620 doi:10.1016/j.epsl.2006.05.034
621 Krief, S., Hendy, E. J., Fine, M., Yam, R., Meibom, A., Foster, G. L., & Shemesh, A. (2010). Physiological and
622 isotopic responses of scleractinian corals to ocean acidification. *Geochimica Et Cosmochimica Acta, 74*(17),
623 4988-5001. doi:10.1016/j.gca.2010.05.023

624 Kubota, K., Yokoyama, Y., Ishikawa, T., Suzuki, A., & Ishii, M. (2017). Rapid decline in pH of coral calcification
625 fluid due to incorporation of anthropogenic CO2. *Scientific Reports (Nature Publisher Group), 7*, 1.
626 doi:10.1038/s41598-017-07680-0
627 Lamberts, A. E. (1978). Coral growth: alizarin method. In D. R. Stoddart, & R. E. Johannes (Eds.), *Coral reefs:*
628 *research methods* (pp. 523-527). Paris: Unesco.
629 Lantz, C., Lantz, C., Atkinson, M., Atkinson, M., Winn, C., Winn, C., . . . Kahng, S. (2014). Dissolved inorganic
630 carbon and total alkalinity of a Hawaiian fringing reef: chemical techniques for monitoring the effects of ocean
631 acidification on coral reefs. *Coral Reefs, 33*(1), 105-115. doi:10.1007/s00338-013-1082-5
632 Martz, T. R., Connery, J. G., & Johnson, K. S. (2010). Testing the Honeywell Durafet® for seawater pH
633 applications. *Limnology and Oceanography: Methods, 8*(5), 172-184. doi:10.4319/lom.2010.8.172
634 McCulloch, M. T., D'Olivo, J. P., Falter, J., Georgiou, L., Holcomb, M., Montagna, P., & Trotter, J. A. (2018).
635 Boron Isotopic Systematics in Scleractinian Corals and the Role of pH Up-regulation. In H. Marshall, & G. L.
636 Foster (Eds.), *Boron Isotopes The Fifth Element* (pp. 145-162). Switzerland: Springer International Publishing
637 AG.
638 McCulloch, M. T., D'olivo, J. P., Falter, J., Holcomb, M., & Trotter, J. A. (2017). Coral calcification in a changing
639 World and the interactive dynamics of pH and DIC upregulation. *Nature Communications, 8*, 15686.
640 doi:10.1038/ncomms15686
641 McCulloch, M., Falter, J., Trotter, J., & Montagna, P. (2012). Coral resilience to ocean acidification and global
642 warming through pH up-regulation. *Nature Climate Change, 2*(8), 623. doi:10.1038/nclimate1473
643 Miller, C. A., Pocock, K., Evans, W., & Kelley, A. L. (2018). An evaluation of the performance of Sea-Bird
644 Scientific's SeaFET ™ autonomous pH sensor: considerations for the broader oceanographic community.
645 *Ocean Science, 14*(4), 751-768. doi:10.5194/os-14-751-2018
646 Mollica, N. R., Guo, W., Cohen, A. L., Huang, K., Foster, G. L., Donald, H. K., & Solow, A. R. (2018). Ocean
647 acidification affects coral growth by reducing skeletal density. *Proceedings of the National Academy of*
648 *Sciences of the United States of America, 115*(8), 1754-1759. doi:10.1073/pnas.1712806115
649 Morrison, R. J., & Woodroffe, C. D. (2009). The Soils of Kiritimati (Christmas) Island, Kiribati, Central Pacific:
650 New Information and Comparison with Previous Studies1. *Pacific Science, 63*(3), 397-411.
651 doi:10.2984/049.063.0308

652 Okai, T., Suzuki, A., Kawahata, H., Terashima, S., & Imai, N. (2002). Preparation of a New Geological Survey of
653 Japan Geochemical Reference Material: Coral JCp-1. *Geostandards Newsletter, 26*(1), 95-99.
654 doi:10.1111/j.1751-908X.2002.tb00627.x
655 R Core Team. (2019). *A language and environment for statistical*
656 *computing*. Vienna, Austria (URL: https://www.R-project.org/):
657 Rae, J. W. B., Foster, G. L., Schmidt, D. N., & Elliott, T. (2011). Boron isotopes and B/Ca in benthic foraminifera:
658 Proxies for the deep ocean carbonate system. *Earth and Planetary Science Letters, 302*(3), 403-413.
659 doi:10.1016/j.epsl.2010.12.034
660 Rhein, M., Rintoul, S. R., Aoki, S., Campos, E., Chambers, D., Feely, R. A., . . . Wang, F. (2013). Observations:
661 Ocean. In T. F. Stocker, D. Qin, G. -. Plattner, M. Tignor, S. K. Allen, J. Boschung, . . . P. M. Midgley (Eds.),
662 *Climate Change 2013: The Physical Science Basis. Contribution of Working Group 1 to the Fifth Assessment*
663 *Report of the Intergovernmental Panel on Climate Change*. Cambridge, United Kingdom and New York, NY,
664 USA: Cambridge University press.
665 Ross, C. L., Falter, J. L., & McCulloch, M. T. (2017). Active modulation of the calcifying fluid carbonate chemistry
666 (δ11B, B/Ca) and seasonally invariant coral calcification at sub-tropical limits. *Scientific Reports, 7*(1), 1-11.
667 doi:10.1038/s41598-017-14066-9
668 Sadekov, A., Lloyd, N. S., Misra, S., Trotter, J., D'Olivo, J., & McCulloch, M. (2019). Accurate and precise
669 microscale measurements of boron isotope ratios in calcium carbonates using laser ablation multicollector-
670 ICPMS. *Journal of Analytical Atomic Spectrometry, 34*(3), 550-560. doi:10.1039/C8JA00444G
671 Scoffin, T. P., Stoddart, D. R., & Rosen, B. R. (1978). The Nature and Significance of Microatolls. *Philosophical*
672 *Transactions of the Royal Society of London. B, Biological Sciences, 284*(999), 99-122.
673 doi:10.1098/rstb.1978.0055
674 Sevilgen, D. S., Venn, A. A., Hu, M. Y., Tambutté, E., de Beer, D., Planas-Bielsa, V., & Tambutté, S. (2019). Full
675 in vivo characterization of carbonate chemistry at the site of calcification in corals. *Science Advances, 5*(1),
676 eaau7447. doi:10.1126/sciadv.aau7447
677 Shaw, E. C., McNeil, B. I., & Tilbrook, B. (2012). Impacts of ocean acidification in naturally variable coral reef flat
678 ecosystems. *Journal of Geophysical Research: Oceans, 117*(C3), n/a. doi:10.1029/2011JC007655

679 Smith, S. V. (1973). Carbon Dioxide Dynamics: A Record of Organic Carbon Production, Respiration, and
680 Calcification in the Eniwetok Reef Flat Community. *Limnology and Oceanography, 18*(1), 106-120.
681 Standish, C. D., Chalk, T. B., Babila, T. L., Milton, J. A., Palmer, M. R., & Foster, G. L. (2019). The effect of
682 matrix interferences on in situ boron isotope analysis by laser ablation MC-ICP-MS. *Rapid Commun Mass*
683 *Spectrom, 33*(10), 959– 968. doi:10.1002/rcm.8432
684 Thil, F., Blamart, D., Assailly, C., Lazareth, C. E., Leblanc, T., Butsher, J., & Douville, E. (2016). Development of
685 laser ablation multi-collector inductively coupled plasma mass spectrometry for boron isotopic measurement in
686 marine biocarbonates: new improvements and application to a modernPoritescoral. *Rapid Communications in*
687 *Mass Spectrometry, 30*(3), 359-371. doi:10.1002/rcm.7448
688 Venn, A., Tambutté, E., Holcomb, M., Allemand, D., & Tambutté, S. (2011). Live Tissue Imaging Shows Reef
689 Corals Elevate pH under Their Calcifying Tissue Relative to Seawater. *PloS One, 6*(5), e20013.
690 doi:10.1371/journal.pone.0020013
691 Wall, M., Fietzke, J., Schmidt, G. M., Fink, A., Hofmann, L. C., de Beer, D., & Fabricius, K. E. (2016). Internal pH
692 regulation facilitates in situ long-term acclimation of massive corals to end-of-century carbon dioxide
693 conditions. *Scientific Reports, 6*, 30688. doi:10.1038/srep30688
694 Walsh, S. M. (2011). Ecosystem-Scale Effects of Nutrients and Fishing on Coral Reefs. *Journal of Marine Biology,*
695 *2011*, 1-13. doi:10.1155/2011/187248
696 Woodroffe, C. D., McGregor, H. V., Lambeck, K., Smithers, S. G., & Fink, D. (2012). Mid-Pacific microatolls
697 record sea-level stability over the past 5000 yr. *Geology, 40*(10), 951. doi:10.1130/G33344.1
698 Woodroffe, C. D., Beech, M. R., & Gagan, M. K. (2003). Mid-late Holocene El Niño variability in the equatorial
699 Pacific from coral microatolls. *Geophysical Research Letters, 30*(7), 1358-n/a. doi:10.1029/2002GL015868
700 Zhang, C., Huang, H., Ye, C., Huang, L., Li, X., Lian, J., & Liu, S. (2013). Diurnal and seasonal variations of
701 carbonate system parameters on Luhuitou fringing reef, Sanya Bay, Hainan Island, South China Sea. *Deep-Sea*
702 *Research. Part II, Topical Studies in Oceanography, 96*, 65-74. doi:10.1016/j.dsr2.2013.02.013

703
704